PROCEEDINGS OF SCIENCE

Geant4 Studies for the HPD-PET scintillators

F. Ciocia,[a] A. Braem,[b] E. Chesi,[b] R. De Leo,[a1] C. Joram,[b] L. Lagamba,[a] E. Nappi,[a] J. Séguinot,[b] I. Vilardi[a] and P. Weilhammer[b]

[a] *Physics Dept. and INFN Section of Bari, Via Orabona 4, Bari, Italy*

[b] *CERN PH-Department, CH-1211 Geneva, Switzerland*

E-mail: deleo@ba.infn.it

In the framework of feasibility studies of the 3D Axial HPD-PET concept, various investigations are being performed about the characteristics of the crystals to be employed. The resolution of the axial reconstruction of a single gamma ray σ_z and its energy σ_E/E depend on the physical and optical properties of the chosen scintillator, including its surface finish, and on the characteristics of the photodetectors. A comparison of computational studies carried out with Geant4 for YAP:Ce crystal bars of dimensions 3.2×3.2×100 mm^3 and experimental results allows to evaluate the influence of the optical parameters of the crystal lateral surfaces on the light collection. We show that a mechanical structuring of the crystal surface, which leads to pure surface absorption, would allow to significantly enhance the PET detector performance.

Frontiers in Imaging Science: High Performance Nuclear Medicine Imagers for Vascular Disease Imaging (Brain and Heart)
Istituto Superiore di Sanita', Rome, Italy
13-14 November, 2006

[1] Speaker.

PoS(FISBH2006)009

1. Introduction

The novel 3D PET geometrical concept [1] is based on axially oriented arrays of long (10-15 cm) and thin polished scintillator bars read out at the two ends by Hybrid Photodetectors (HPD) [2]. The concept allows for an unambiguous reconstruction of the photon's interaction point eliminating the Depth of Interaction (DoI) uncertainty. The axial coordinate *z* is obtained from the ratio of the light quantity at the two crystal ends. The resolutions of the axial *z* coordinate (σ_z), the gamma ray energy (σ_E/E), and the detection time (σ_T) of the device are influenced [1,3] by λ_{eff} and N_0, the key parameters of the HPD-PET concept. The effective light attenuation length λ_{eff} describes the absorption of photons along their path inside the crystal. λ_{eff} is smaller than the bulk absorption length λ_{bulk} as it relates to the projected axial path length. N_0 is the number of photoelectrons (*pe*'s) detected for a 511 keV γ-ray in a crystal bar without any light absorption ($\lambda_{eff} = \infty$). Its value depends both on the physical and optical properties of the chosen scintillator and of its surface, and on the characteristics of the photodetector. While an increase of N_0 improves the resolution of all 3 quantities (*z*, *E*, *t*), a longer λ_{eff} improves σ_E/E and σ_T, however it worsens σ_z. The best compromise for λ_{eff} was predicted [1] by the simulations to be about 2/3 of the crystal length L_c.

A recent experimental study [3] with a set of polished YAP:Ce scintillators of dimensions 3.2×3.2×100 mm^3 focused on methods of adjusting λ_{eff} by wrapping the bars with Teflon or by coating the crystal lateral surfaces with very thin metallic layers. In this paper, we simulate the optical processes in the crystal bars with Geant4 [4]. The comprehension of the influence of the optical properties of the crystal surfaces on the light collection is an essential ingredient to optimize the detector performance.

2. The HPD-PET Concept

The axial HPD-PET concept assumes that the measured *pe* yields N_1 and N_2 at the bar ends vary exponentially with the average path length of the scintillation light. For a single 511 keV γ-ray:

$$N_1 = ½ \cdot N_0 \cdot \exp\frac{-z}{\lambda_{eff}}, \qquad N_2 = ½ \cdot N_0 \cdot \exp\frac{-(L_C - z)}{\lambda_{eff}}, \tag{1}$$

$$N_{pe}(z) = N_1 + N_2, \tag{2}$$

with N_{pe} being the total number of detected photoelectrons.

The axial coordinate *z* of the interaction point is derived from the relation:

$$z = \frac{1}{2}\left(\lambda_{eff} \ln \frac{N_1}{N_2} + L_C\right) \tag{3}$$

and its uncertainty, taking into account only the statistical error on $N_{1,2}$, is:

$$\sigma_z = \frac{\lambda_{eff}}{\sqrt{2N_o / ENF}}\left(\exp\frac{z}{\lambda_{eff}} + \exp\frac{L_C - z}{\lambda_{eff}}\right)^{1/2}. \tag{4}$$

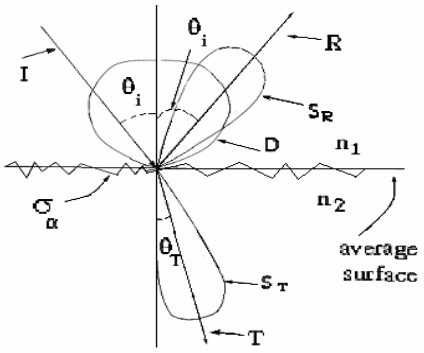

Figure 1. Schematic polar plot of the possible processes at the interface between the crystal (n_1) and the coated (or wrapped) lateral surface (n_2). Absorption (A) is not indicated in the figure.

The energy and time resolutions are respectively:

$$\frac{\sigma_E}{E} = \sqrt{\frac{ENF}{N_{pe}}} \oplus R_{\text{int}}, \qquad \sigma_T = \frac{c}{\sqrt{N_{pe}}} \oplus c'. \tag{5}$$

In the previous equations, *ENF* is the excess noise factor [3] of the photodetector, R_{int} the intrinsic resolution of the scintillator, and c and c' are constants to be determined experimentally. These equations clearly explicit that an increase of N_0 improves all the resolutions, while an increase of λ_{eff}, although improving σ_E/E and σ_T, worsens σ_z.

3. Geant4 simulations

We discuss in this section the various optical parameters used in the Geant4 code to describe the light collection and their influence on the resolutions σ_z, σ_E/E.

For the simulations we assumed YAP crystals with the following intrinsic properties: light yield N_{ph} = 18/keV, intrinsic energy resolution σ_E/E_{int} = 2.4%, refractive index n_1 = 1.94 at 370 nm. The bar lateral surface was assumed surrounded by air, or with a fraction (f_2) wrapped with a n_2 material, or coated. In this last case a complex refractive index (n_2, k_2) of the thick (t) coating is assumed. The PMTs coupled to the bar polished bases were simulated with a borosilicate window with a refractive index n_w = 1.474, an *ENF* of 1.2, and a quantum efficiency ε_Q = 0.25.

At each photon impact on the crystal lateral surfaces the following optical processes were considered [5] (see figure 1): absorption (A), transmission (T), reflection (R), diffusion (D), with a Lambertian distribution, and a possible smearing (S), i.e. a reflection S_R or a transmission S_T when the normal to the local surface is rotated with respect to that of the average crystal surface. In this last case the rotation angle was randomly chosen from a Gaussian distribution with dispersion σ_α. The backscattering was disregarded. Obviously, $A + R + T + D + S_{R,T} = 1$. A and D were varied independently of n_1 and n_2, the refractive indices of the crystal and its coating (or air). The reflection and transmission coefficients R and T, or S_R and S_T, were calculated according to the Fresnel relations assuming random polarization of the incident photons.

A polished crystal in air is simulated with $n_2 = n_{air} = 1$, $\sigma_\alpha = D = A = 0$. For a diffusive n_2 wrapping we chose $\sigma_\alpha = 0$, $D \neq 0$, $A \neq 0$, and for a roughened crystal surface $n_2 = 1$, $\sigma_\alpha \neq 0$.

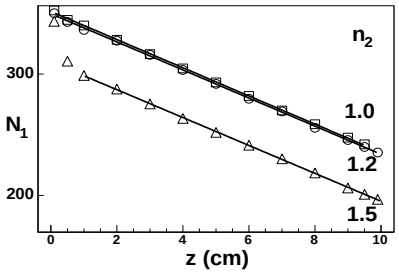

Figure 2. Photoelectrons N_1 detected on one bar end for scintillation at different *z*-positions in a polished YAP with a wrapping of the lateral surface with the indicated refractive indices. The lines are fits to the points according to eq. 1.

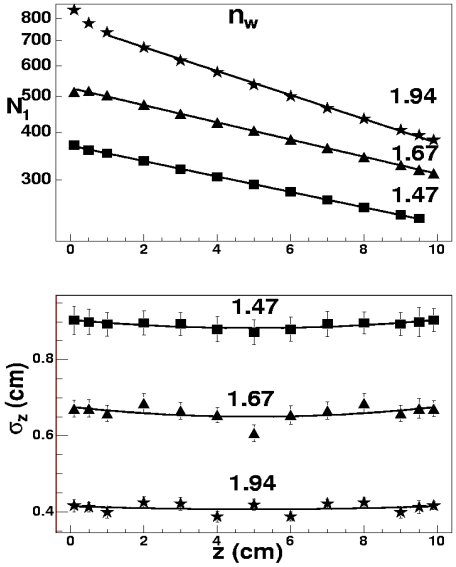

Figure 3. Photoelectrons N_1 detected on one bar end (upper panel) and *z*-resolution (lower panel) for scintillations at different *z*-positions in a YAP bar. The lateral surfaces are polished ($n_2 = 1$). The different datasets correspond to photodetectors with different refractive indices of the window. The lines are fits to the points with eq. 1 in the upper panel and with eq. 4 in the lower one.

The transmission of the scintillation light to the photodetector depends on the limit angle at the interface crystal-window $\theta_a = \sin^{-1}(n_w/n_1)$.

In long and thin crystals bars two components are transmitted to the photodetector:

The direct component (the fraction of detected photons without reflections on the crystal lateral surfaces), dominant for scintillations at short distances from the window, is:

$$f(\theta_a) = \frac{1}{4\pi} \cdot 2\pi \cdot \int_0^{\theta_a} \sin\theta \, d\theta = \frac{1}{2} \cdot [1 - \cos\theta_a] \tag{6}$$

where $\theta \leq \theta_a$ is defined by the distance to the PMT window.

The number of detected photoelectrons is

$$N_{0a} = N_{ph} \cdot f(\theta_a) \cdot \varepsilon_Q. \tag{7}$$

The indirect component is the fraction of photons which propagates in the crystal bar by total internal reflection. It is limited to polar angles in the range from 0 to $\pi/2 - \theta_b$ with $\theta_b = \sin^{-1}(n_2/n_1)$ measured with respect to the normal of the window. The yield of the indirect component

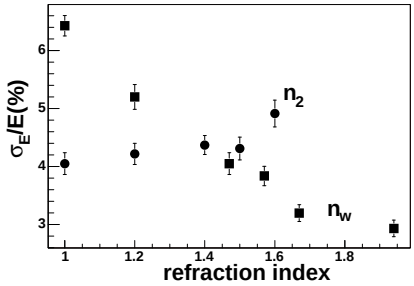

Figure 4. Relative energy resolution, measured for 511 keV γ-rays detected in the centre of a YAP crystal long 10 cm, versus the refractive index of its lateral surface wrapping (circles), and of the photodetector windows (squares).

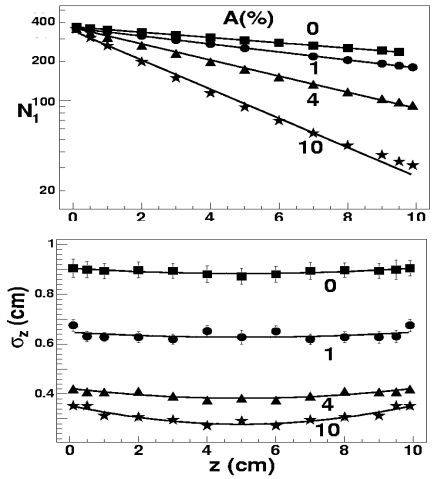

Figure 5. Photoelectrons N_1 detected (upper panel) at one bar end (photodetector with n_w = 1.47) and uncertainty of *z*-reconstruction (lower panel) for scintillations at different *z*-positions in a YAP bar with polished lateral surface (n_2 = 1). The absorption parameter has been varied as indicated.

$$N_{0a} = N_{ph} \cdot f\left(\frac{\pi}{2} - \theta_b\right) \cdot \varepsilon_Q \tag{8}$$

decreases when n_2 increases, i.e when a coating is used.

However, for $1 < n_2 \leq 1.25$, although the intensity of the indirect component decreases, the limiting factor is still the transmission at the PMT borosilicate window and the overall yield is therefore unchanged (see figure 2). On the contrary, for higher values of n_2 (1.5 in figure 2) the loss of light arriving at the end of the bar is dominant.

The behaviour is completely different with a sapphire window (n_w = 1.793). The transmitted photon flux starts to decrease when as soon as n_2 is larger than 1.

As shown in figure 2 λ_{eff} is independent of n_2. However one observes at small distances a slight deviation from an exponential due to the detection of the direct component.

The influence of n_w on N_1 and σ_z for polished crystals in air is shown in figure 3. As previously quoted N_0 increases with n_w up to a maximum value attained when the crystal-window refractive indices are perfectly matched. A reduction of the effective attenuation length λ_{eff} (upper panel of the figure) is observed which leads to a significant improvement of the resolution σ_z (lower panel of figure 3).

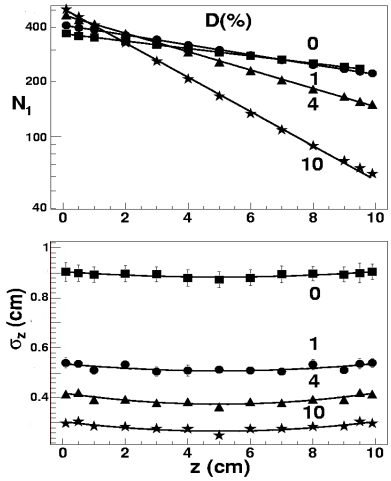

Figure 6. Photoelectrons N_1 detected (upper panel) on one bar end (photodetector with n_w = 1.47) and uncertainties in the scintillation position reconstruction (lower panel) for scintillations at different *z*-positions in a YAP bar with the lateral surface (n_2 = 1) polished and diffusing the indicated percentages of the optical photon flux.

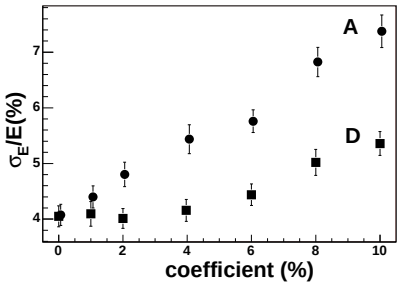

Figure 7. Relative energy resolution, measured for 511 keV γ-rays impinging in the centre of a 10 cm long YAP crystal, versus the percentages of the photon flux undergoing absorption (full points) or diffusion (full squares).

The energy resolution for gammas interacting at the crystal centre ($z = L_C/2$ = 5 cm) reported in figure 4 clearly gets worse for increasing values of n_2 (full circles), and decreasing n_w values (full squares).

The influence of the absorption (*A*) on N_1 and σ_z is displayed in figure 5. Increasing *A* does not reduce N_0 but lowers λ_{eff}, improving σ_z which, however, gets saturated above 10%. These results, obviously, would improve with a sapphire window.

The consequences of the diffusion (*D*) on N_1 and σ_z are shown in figure 6. These are similar to those of the absorption but with an increase of N_0. This is due to photons with polar angles above the limit angle at the interface that are lost in a polished crystal, but can acquire after diffusion a lower polar angle and, thus, be detected. For this reason, transport efficiencies greater than those calculated with eq. 6 can be obtained. The σ_z improvement due to absorption and diffusion is counter-balanced with a worsening of the energy resolution, as observed in figure 7 for gammas interacting at the crystal centre. However the degradation is reduced with a diffusive coating due to the increase of N_0 .

As shown in figure 8, the angular smearing effect destroys the exponential dependence of N_1 on the *z* coordinate which is a requirement for the coordinate reconstruction by means of eq. 3. Such an effect would seriously compromise the performance of the HPD-PET concept.

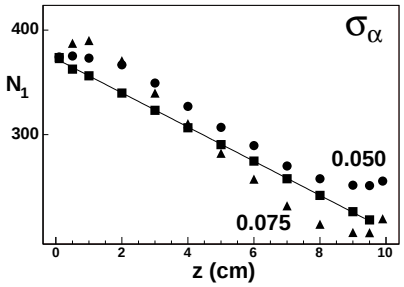

Figure 8. Photoelectrons N_1 detected in one side photodetector ($n_w = 1.47$) for scintillations at different *z*-positions in a YAP bar with the lateral surface ($n_2 = 1$) smeared (dots, triangles) with the indicated σ_α (in rad) angles. Squares (fitted with the solid line) refer to a polished (not smeared) surface.

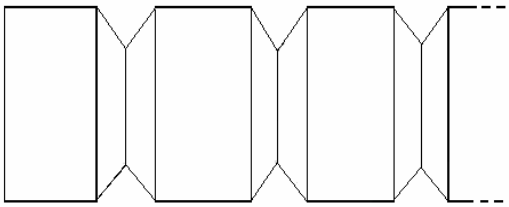

Figure 9. Engravings on the lateral surface of a polished crystal (not to scale). Their number (from 10 to 100 per cm) and depth (from 50 to 100 μm) can be used to tune the absorption of the internal transmitting photon flux.

No variation of the N_0 and λ_{eff} values has been found by varying the crystal cross section and its length L_c for polished YAP crystals in air coupled to a PMT with a borosilicate window.

However, an increase of the length worsens the resolution σ_z in agreement with Eq. 4 for a constant λ_{eff} value.

The simulations suggest that a low percentage of photons undergoing Lambertian diffusion (obtainable, for example, with a partial roughening of the lateral surfaces) is a good approach to improve σ_z. However, such a technique would be very challenging in view of a good reproducibility for the production of a large quantity of bars.

A very promising and practical method to obtain the required [1] performances seems a geometry related absorption of the lateral surfaces of the crystal bar. It could be implemented by triangular engravings (cuts) applied to the lateral surfaces of the polished crystal bars (see figure 9). The absorption probability *A* is driven by the number of cuts and their depth. Various patterns have been simulated with Geant4. Technically, the pattern can be produced by laser etching followed by a chemical polishing [6].

Figure 10 illustrates the performance which can be achieved for different parameters of the engraving. The method maintains the relation $N_1(z)$ perfectly exponential. In contrast to all other methods it allows to significantly improve σ_z while σ_E/E is practically unaffected. The resolutions are almost constant over the full bar length. A PET scanner with this performance would be a very competitive device.

4. Conclusions

In this paper we have discussed Geant4 simulations of the long and thin scintillator crystals bars to be used for the axial HPD-PET project.

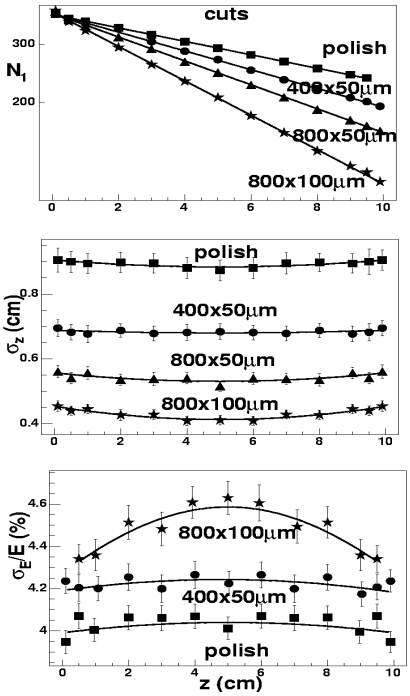

Figure 10. Photoelectrons N_1 detected (upper panel) at one bar end (photodetector with n_2 = 1.47) and uncertainties of the *z* (middle panel) and energy (lower panel) reconstruction as a function of the *z* scintillation point. The lateral polished surfaces are engraved with different patterns varying in number and depth of the cuts.

These simulations have shown that the best matching of the refractive indices of crystal and the photodetector windows is, as expected, paramount to optimize the detected light yield, and consequently the energy and position resolution of the single gamma ray.

The various tested wrapping/coatings of the crystal lateral surface have contrasting results on the resolutions. Their behaviour is reproduced by the Geant4 simulations and accounted for by the parameters N_0 and λ_{eff}, which are the key values characterizing the system crystal bar - photodetector.

The various optical parameters involved in the propagation of the photon flux have been parameterized and their respective contributions to the resolutions revealed by the simulations.

It appears that the best possible way to optimize the detector performances is to realize a controlled absorption of the crystal surfaces. An engraving technique has been proposed using laser etching and chemical polishing.

References

[1] J. Seguinot et al., *Novel Geometrical Concept of High Performance Brain PET Scanner –Principle, Design and Performance Estimates*, CERN PH-EP/2004-050, *Il Nuovo Cimento* ***29C*** (2006) 429.

[2] C. Joram, *Hybrid Photodiodes, Nucl. Phys. B (Proc. Supp.)* **7** (1999)407, E. Chesi et al., *A segmented Hybrid Photon Detector withintegrated auto-triggering front-end electronics for a PET scanner, Nucl. Instrum. Meth.* **A564** (2006) 352.

[3] I. Vilardi et al., *Optimization of the effective light attenuation length of YAP:Ce and LYSO:Ce crystals for a novel geometrical PET concept, Nucl. Instrum. Meth.* **A564** (2006) 506.

[4] geant4.web.cern.ch, S. Agostinelli, et al., *GEANT4-a simulation toolkit, Nucl. Instrum. Meth.* **506** (2003) 250; M.G. Pia, *The Geant4 Toolkit: simulation capabilities and application results, Nucl. Phys. B - Proc. Suppl.* **125** (2003) 60.

[5] A. Levin, C. Moisan, *A more physical approach to model the surface treatment of scintillation counters and its implementation into DETECT*, IEEE Nucl. Sci. Symposium, Anaheim Oct. 1996, TRI-PP-96-64.

[6] V.V. Nagarkar, et al., *A high efficiency pixilated detector for small animal PET*, University of California, Paper 178, 2004.